Photoemission Properties of Simple Metals*

Richard Y. Koyama†

Stanford Electronics Laboratory, Stanford University, Stanford, California 94305

and

Neville V. Smith

Bell Telephone Laboratories, Murray Hill, New Jersey 07974‡ and
Stanford University, Stanford, California 94305

(Received 22 June 1970)

The predictions of the nearly free-electron model for the photoemission properties of simple metals are derived and applied to the available data on K, Ag, and Al. The optical transitions are taken to be direct. The energy distribution curve (EDC) of photoemitted electrons is then related to the energy distribution of the joint density of states (EDJDOS). In the one- and two-orthogonalized-plane-wave (OPW) approximations, the EDJDOS is predicted to be rectangular in shape with a width which increases quadratically with photon energy. The experimental data on K and on the "$L_{2'} \rightarrow L_1$" transitions in Ag show some agreement with this result. In the case of Al, the EDJDOS has been calculated numerically using Ashcroft's four-OPW band structure. The over-all rectangular features can still be discerned, but there is much additional structure due to the inclusion of the extra OPW's. The EDC's for Al at several photon energies are calculated by introducing appropriate threshold factors and are found to agree reasonably well with the data of Wooten *et al.* Only the three uppermost peaks in the theoretical EDJDOS are presently accessible to experiment, and these correspond fairly closely in energy with the three peaks in the density of states. The implications with regard to the alternative nondirect interpretation are discussed.

I. INTRODUCTION

The nearly free-electron model has proved quite successful in explaining many of the electronic properties of metals. In this paper we survey the extent to which the model can account for the photoemission properties of simple metals. The predictions of the model for the optical absorption have been derived by Wilson,[1] and have been applied to the alkali metals by Butcher.[2] Since the advent of the pseudopotential formalism, there has been renewed interest in the nearly free-electron interpretation of optical experiments as a means of determining the magnitudes of pseudopotential coefficients. The work of Golovashkin, Kopeliovich, and Motulevich[3] is particularly relevant. This paper represents a systematic attempt to extend the foregoing ideas to a prediction of the photoemission properties of a nearly free-electron metal. The extension is straightforward but is believed to be of some importance in view of the rapid growth of the photoemission technique as a means of determining band structure. It is desirable to test the reliability of the photoemission technique on simple metals, i.e., materials where one thinks one knows the band structure in advance.

We will work within the prevailing "three-step" model, in which the photoemission process is envisaged as three independent steps: (1) optical excitation of electrons in the interior of the material,

(2) transport of some of these electrons to the surface, and (3) escape of some of these electrons across the surface to be detected as photoelectrons. Steps (2) and (3) have been treated elsewhere[4,5] and our concern will be with step (1), the optical excitation. Within the one-electron approach adopted here, the optical transitions will be considered to be direct, i.e., the initial and final states must lie at the same point in $\vec{k}$ space in the reduced zone scheme. The alternative nondirect approach[5,6] in which conservation of $\vec{k}$ is regarded as unimportant would take us beyond any simple theory, although it will be discussed briefly in Sec. V.

In Sec. II, we introduce the key concept of the energy distribution of the joint density of states (EDJDOS) and discuss its relation to the experimental energy distribution curves (EDC's) of photoemitted electrons. We then go on to consider cases of increasing complexity. Section III is concerned with the EDJDOS for perfectly free-electron bands, or what, in Harrison's terminology,[7] would be called the one-orthogonalized-plane-wave (OPW) approximation. It will be shown that the EDJDOS in this case is rectangular in shape, i.e., at a given photon energy $\hbar\omega$, the EDJDOS is constant between an upper and lower energy cutoff and is zero outside. The rectangular box shape will be a recurrent theme throughout the paper. The predictions for perfectly free-electron bands will be compared with recent data on K taken by Smith and

Spicer.[8]

Section IV deals with the two-OPW approximation. It is found that the EDJDOS is once again rectangular-box shaped. The results are applied to experimental EDC's on Ag. While Ag does not strictly classify as a simple metal, the energy surfaces in the vicinity of the $L_2 \rightarrow L_1$ band gap can be expressed fairly well with two OPW's. We will therefore consider only transitions in the vicinity of $L_2 \rightarrow L_1$. Transitions from the low-lying d bands fall beyond the scope of our present discussion.

Section V treats the four-OPW approximation and applies it to Al. The algebra becomes too cumbersome at this stage and so we have resorted to numerical techniques. The gross features of the EDJDOS for Al are similar to those for the one- and two-OPW methods in that over-all rectangular shape can be discerned. However, there is much additional structure due to the inclusion of the additional OPW's. This structure will be compared with the experimental data of Wooten, Huen, and Stuart.[9] It will be seen that there is reasonable agreement.

II. DEFINITION OF TERMS

A. Joint Density of States

Conventional interband transitions can take place only between initial and final states which lie at the same point in $\vec{k}$ space in the reduced zone scheme. These are known as direct or vertical transitions. If $\mathcal{E}_i(\vec{k})$ and $\mathcal{E}_f(\vec{k})$ denote energies in an initial band i and a final band f, respectively, then transitions between these two bands at photon energy $\hbar\omega$ are restricted to the surface of constant interband energy given by

$$\Omega_{fi}(\vec{k}) = \mathcal{E}_f(\vec{k}) - \mathcal{E}_i(\vec{k}) - \hbar\omega = 0. \qquad (1)$$

A quantity related to the optical absorption is the joint density of states (JDOS) defined by

$$\mathcal{J}(\hbar\omega) = (2\pi)^{-3} \sum_{i,f} \int' d^3k\, \delta(\Omega_{fi}(\vec{k})). \qquad (2)$$

The prime on the integral denotes that the integration is to be performed only over those portions of $\vec{k}$ space for which $\mathcal{E}_f > E_F > \mathcal{E}_i$, where E_F is the Fermi energy. The summation is performed over all pairs of bands. The JDOS therefore represents the total number of direct transitions which can take place at the photon energy $\hbar\omega$.

Photoemission experiments, however, measure not just the total number of transitions, but also how the optically excited electrons are distributed in energy. We therefore introduce a quantity called (EDJDOS) defined by the energy distribution of the joint density of states

$$\mathfrak{D}(\mathcal{E}, \hbar\omega) = (2\pi)^{-3} \sum_{i,f} \int' d^3k\, \delta(\Omega_{fi}(\vec{k}))\, \delta\,(\mathcal{E} - \mathcal{E}_i(\vec{k})). \qquad (3)$$

The extra δ function picks out those transitions whose initial states lie at energy $\mathcal{E}$. Note that in Eqs. (2) and (3), each transition is counted with equal weight. If we wish to relate to any physically observable quantities, we should weight each transition with the square of a momentum matrix element. In what follows, however, we will be working in a constant matrix element approximation, so that we may use Eqs. (2) and (3) as they stand.

It is possible to integrate over the δ functions in Eqs. (2) and (3) and express the JDOS and the EDJDOS in more elegant form. The JDOS of Eq. (2) reduces to the well-known form[10]

$$\mathcal{J}(\hbar\omega) = (2\pi)^{-3} \sum_{i,f} \int' (dS_{fi}/|\nabla_{\vec{k}} \mathcal{E}_f - \nabla_{\vec{k}} \mathcal{E}_i|), \qquad (4)$$

the integral being carried out over the surface $\Omega_{fi}(\vec{k}) = 0$. By an exactly analogous manipulation,[11] the expression for the EDJDOS may be converted to a line integral:

$$\mathfrak{D}(\mathcal{E}, \hbar\omega) = (2\pi)^{-3} \sum_{i,f} \int' (dl_{fi}/|\nabla_{\vec{k}} \mathcal{E}_f \times \nabla_{\vec{k}} \mathcal{E}_i|). \qquad (5)$$

The integral is performed around the line of intersection of the two constant energy surfaces $\mathcal{E}_i = \mathcal{E}$ and $\mathcal{E}_f = \mathcal{E} + \hbar\omega$.

B. Photoemitted Electrons

In a constant matrix element approximation, the EDJDOS, $\mathfrak{D}(\mathcal{E}, \hbar\omega)$ represents the energy distribution of photoexcited electrons referred to initial-state energy $\mathcal{E}$. Of course, the photoelectrons emerge with energy equal to the final energy $E = \mathcal{E} + \hbar\omega$. To obtain the EDC for photoemitted electrons, we must take account of the transport to the surface and the escape across it. Following Berglund and Spicer,[5] we simply multiply the EDJDOS by an appropriate escape probability $T(E, \hbar\omega)$. The EDC is then given by

$$\mathfrak{N}(E, \hbar\omega) = C\, T(E, \hbar\omega)\, \mathfrak{D}(E - \hbar\omega, \hbar\omega). \qquad (6)$$

C is a normalizing constant and $T(E, \hbar\omega)$ is given by

$$T(E, \hbar\omega) = T_0(E)\left[1 - \frac{1}{\alpha l T_0(E)}\, \ln\left(\frac{\alpha l + 1}{1 + \alpha l - 2\alpha l T_0(E)}\right)\right], \qquad (7)$$

$$T_0(E) = \tfrac{1}{2}\{1 - [(E_F + e\varphi)/E]^{1/2}\}, \quad E > E_F + e\varphi,$$
$$T_0(E) = 0, \qquad\qquad\qquad\qquad E \leq E_F + e\varphi. \qquad (8)$$

In these expressions, E is measured from the bot-
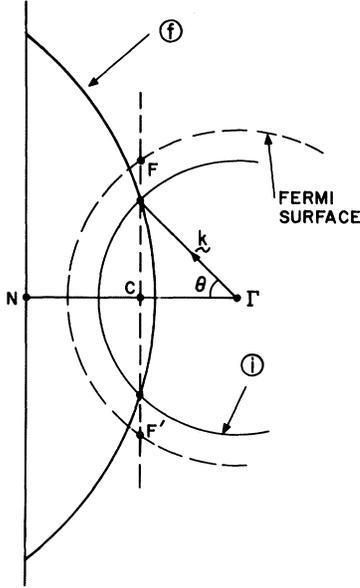
FIG. 1. Geometry of the constant energy surfaces for optical transitions at photon energy $\hbar\omega$ between perfectly free-electron bands. Γ is the origin of k space and N is the center of the zone boundary generated by the vector $\vec{G}$. The vertical dashed line represents the plane of constant interband energy, and the spheres labeled i and f correspond to the surfaces $\mathcal{E}_i = \mathcal{E}$ and $\mathcal{E}_f = \mathcal{E} + \hbar\omega$. Direct transitions are permitted only for states lying on the disk whose diameter is represented by FCF'.

tom of the free-electron band, and $e\varphi$ is the work function; α is the optical absorption coefficient and depends on ω; l is a mean free path which takes account of loss of electrons by inelastic electron-electron scattering and varies strongly with E.

III. ONE-OPW: ALKALI METALS

For simple monovalent metals such as the alkali metals, the occupied states lie well within the first zone. We may ignore the gaps at the zone boundaries and use the perfectly free-electron (or one-OPW) form for the initial and final energies

$$\mathcal{E}_i(\vec{k}) = \beta k^2, \qquad \mathcal{E}_f(\vec{k}) = \beta(\vec{k} + \vec{G})^2, \tag{9}$$

where $\beta = \hbar^2/2m$ and $\vec{G}$ is the reciprocal-lattice vector which generates the fth band. The surface of constant interband energy at $\hbar\omega$ is the plane

$$\beta(2\vec{k} \cdot \vec{G} + G^2) - \hbar\omega = 0. \tag{10}$$

The surfaces $\mathcal{E}_f = \mathcal{E} + \hbar\omega$ and $\mathcal{E}_i = \mathcal{E}$ are simply spheres indicated, respectively, by the circled f and i in Fig. 1. The integral of Eq. (5) is performed around the circle of intersection of these two spheres. The vector product in the denominator of the integral is given by

$$\left| \nabla_{\vec{k}} \mathcal{E}_f \times \nabla_{\vec{k}} \mathcal{E}_i \right| = 4\beta^2 \left| \vec{k} \times \vec{G} \right|. \tag{11}$$

If $\mathfrak{D}_{fi}(\mathcal{E}, \hbar\omega)$ denotes the contribution to $\mathfrak{D}(\mathcal{E}, \hbar\omega)$ from this pair of bands, it follows, using the nomenclature of Fig. 1, that

$$\mathfrak{D}_{fi}(\mathcal{E}, \hbar\omega) = \frac{(2\pi)^{-3}}{4\beta^2} \int \frac{dl_{fi}}{kG \sin\theta}. \tag{12}$$

By cylindrical symmetry about the line ΓN, θ and k are constant around the line of integration, so that

$$\mathfrak{D}_{fi}(\mathcal{E}, \hbar\omega) = \frac{(2\pi)^{-3} 2\pi k \sin\theta}{4\beta^2 kG \sin\theta} = \frac{(2\pi)^{-2}}{4\beta^2 G}. \tag{13}$$

It is seen that the k and θ dependence cancel out, leaving a constant height for $\mathfrak{D}(\mathcal{E}, \hbar\omega)$. There are, however, upper and lower bounds on $\mathcal{E}$. The maximum value E_{max} is fixed at E_F by the Fermi cutoff (the Fermi surface is indicated as a dashed curve in Fig. 1). Only those initial states on the portion of the plane of constant interband energy lying inside the Fermi sphere satisfy $\mathcal{E}_i < E_F$. This constitutes a disk of permitted states whose diameter is represented by the line FCF' in Fig. 1.

The minimum initial energy E_{min} corresponds to the situation where the sphere $\mathcal{E}_i = \mathcal{E}$ and $\mathcal{E}_f = \mathcal{E} + \hbar\omega$ just touch. This occurs at the point at the center of the plane of constant interband energy, labeled C in Fig. 1. The energy at C is readily evaluated. The extremal energies are given by

$$E_{min} = (\hbar\omega - \beta G^2)^2/4\beta G^2, \quad E_{max} = E_F. \tag{14}$$

Summing over all equivalent $\vec{G}$ vectors, we obtain

$$\mathfrak{D}(\mathcal{E}, \hbar\omega) = \begin{cases} \text{const}, & E_{min} < \mathcal{E} < E_{max} \\ \\ 0, & \text{elsewhere}. \end{cases} \tag{15}$$

This is the predicted rectangular-box shape for the EDJDOS. The result has been derived previously by Methfessel[12] and by Mayer and Thomas[13] in a way which avoids the line integral.

An important result is that E_{max} is constant, whereas E_{min} is quadratic with photon energy. The width of the energy distribution $(E_{max} - E_{min})$ is therefore expected to vary with photon energy. This prediction is tested against experiment in Fig. 2 which shows some recent EDC's on K taken by Smith and Spicer.[8] A peak is observed at the high-energy end of the experimental EDC's. The theoretical EDJDOS is represented by the dashed rectangles. It is seen that the experimental peak falls within the correct energy range and increases in width with increasing photon energy; the full circles on the experimental curves represent the estimated

position of the valley in the EDC's. For conve-
nience, we will define this as the low-energy de-
marcation of the peak.

The results for K at a number of photon energies
are summarized in Fig. 3, where we have plotted
the position of the valley as a function of photon en-
ergy. Here, we have chosen to refer the electron
energies to the initial states of the optical transi-
tions. In other words, if E_v represents the elec-
tron kinetic energy at a valley position in Fig. 2,
then the full circles in Fig. 3 represent $E_v - \hbar\omega$
$+ e\phi$. This choice of scale places the zero of ener-
gy at the Fermi energy. The open circles in Fig. 3
represent points of inflection in the experimental
EDC's at low photon energies where the valley is
not fully developed. Also shown in Fig. 3 are the
predicted curves for E_{min} for the $\langle 110 \rangle$ and $\langle 200 \rangle$
reciprocal-lattice vectors calculated from Eq. (14).
The valley positions fall close to the curve for
$E_{min}(110)$, indicating that the variation of the width
of the leading peak is well understood in terms of
the nearly free-electron model. Returning to Fig.
2, however, we see that the shape of the leading
peak is not so successfully explained. It remains
to be seen whether this is due to a deficiency in the
experiments or a breakdown of the model. The
behavior in Na, [8] and Rb and Cs [14] has been found
to be very similar to that in K.

IV. TWO-OPW: $L_{2'} \rightarrow L_1$ TRANSITIONS IN SILVER

If the band gaps at the zone boundaries are not
small, we must take explicit account of the distor-

FIG. 3. Comparison of the theoretical values for E_{min}
for K (full curves) with the positions of the valley minima
in the experimental data (full circles). The Fermi level
is taken as the zero of energy.

tions of the energy surfaces from sphericity. In
the two-OPW approximation, Eqs. (9) are simply
replaced by[15]

$$2\mathcal{E}_i(\vec{k}) = \beta[(\vec{k} + \vec{G})^2 + \vec{k}^2] - \{\beta^2[(\vec{k} + \vec{G})^2 - \vec{k}^2]^2 + 4V_G^2\}^{1/2},$$

$$2\mathcal{E}_f(\vec{k}) = \beta[(\vec{k} + \vec{G})^2 + \vec{k}^2] + \{\beta^2[(\vec{k} + \vec{G})^2 - \vec{k}^2]^2 + 4V_G^2\}^{1/2},$$

$$(16)$$

where V_G is the Gth Fourier component of the pseu-
dopotential. The surface of constant interband en-
ergy is given by

$$\beta(2\vec{k} \cdot \vec{G} + G^2) - [(\hbar\omega)^2 - 4V_G^2]^{1/2} = 0 . \quad (17)$$

As in the one-OPW approximation, this surface is
a plane which lies parallel to the zone boundary.
The geometry of this plane and the surfaces $\mathcal{E}_i = \mathcal{E}$
and $\mathcal{E}_f = \mathcal{E} + \hbar\omega$ is illustrated schematically in
Fig. 4. Elementary differentiation of Eq. (16)
leads to

$$|\nabla_{\vec{k}}\mathcal{E}_f(\vec{k}) \times \nabla_{\vec{k}}\mathcal{E}_i(\vec{k})| = 4\beta^2(1 - \gamma)|\vec{k} \times \vec{G}| , \quad (18)$$

where

$$\gamma = 1 - [(\hbar\omega)^2 - 4V_G^2]^{1/2}/\hbar\omega . \quad (19)$$

Proceeding as before, we may invoke cylindrical
symmetry about the line ΓL in Fig. 4 to obtain

$$\mathcal{D}_{fi}(\mathcal{E}, \hbar\omega) = (2\pi)^{-2} 4\beta^2 G(1 - \gamma) . \quad (20)$$

This is once again a rectangular-box-shaped dis-
tribution with the height modified by the factor
$(1 - \gamma)^{-1}$. The low-energy cutoff corresponds to the
point C in Fig. 4. The extremal energies are,
therefore,

$$E_{min} = [(\hbar\omega - \beta G^2)^2 - 4V_G^2] / 4\beta G^2 ,$$

$$E_{max} = E_F . \quad (21)$$

FIG. 2. The high-energy end of the experimental EDC's
on K plotted against kinetic energy $E - (E_F + e\varphi)$ of the
photoelectrons. The dashed rectangles represent the
EDJDOS for perfectly free-electron bands referred to
final states. The heights of the rectangles have been ad-
justed to match the heights of the experimental peaks.

As in the one-OPW case, the width of the box varies quadratically with photon energy.

A word here on optical matrix elements would be appropriate. If ψ_i and ψ_f denote the wave functions associated with the eigenenergies of Eq. (16), the optical transition strength is given by $|\langle \psi_i | \vec{\nabla} | \psi_f \rangle |^2$, the square of the momentum matrix element. It is easily shown[16] that

$$| \langle \psi_i | \vec{\nabla} | \psi_f \rangle |^2 = G^2 |V_G|^2 / (\hbar\omega)^2 . \tag{22}$$

Note that the matrix element is independent of $\mathcal{E}_i$, $\mathcal{E}_f$, or $\vec{k}$, insofar as V_G is independent of these parameters. This provides useful justification for our use of constant matrix elements.

Let us apply these results to Ag. Taking $\vec{G}$ as the $\langle 111 \rangle$ reciprocal-lattice vector, we have $\beta G^2 = 27$ eV. The $L_{2'}$ to L_1 band gap is known from piezoreflectance work by Morris and Lynch[17] to be 4.15 eV. This gives us our value for $2V_G$. Morris and Lynch also find that $L_{2'}$ is 0.30 eV below the Fermi level. We therefore have all the parameters required to determine the form of the EDJDOS from Eqs. (20) and (21). Figure 5 shows an experimental EDC taken by Bauer[18] on heat-cleaned bulk Ag. The rectangular box represents the calculated EDJDOS (the height was chosen arbitrarily). It can be seen that there is some structure in the experimental EDC which corresponds quite well to the
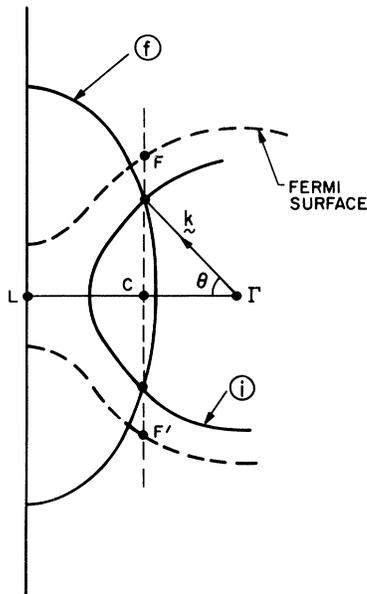
FIG. 5. The experimental EDC at $\hbar\omega = 10.2$ eV obtained by Bauer (Ref. 18) on heat-cleaned Ag. The energy scale is the kinetic energy $E - (E_F + e\varphi)$ of the photoelectrons. The dashed rectangular box represents the theoretical EDJDOS referred to final states.

theoretical rectangular box. The large peak with its edge near 1.5 eV is due to electrons from the d bands. These lie beyond the scope of this paper. We confine ourselves to the conduction-band-to-conduction-band transitions at the high-energy end of the EDC.

The same rectangular box can be seen in the EDC's on cesiated Ag taken by Berglund and Spicer.[5,19] In Fig. 6 we show the high-energy end of the EDC's on cesiated Ag for several photon energies. Again we plot the electron energies with respect to their initial states. The dashed lines represent a somewhat conjectural estimate of the background.[20] The cross-hatched areas produced in this way exhibit the characteristic rectangular shape. Also, the width of the box increases with photon energy, as expected. The full circles indicate the estimated position of the valley minima and the open circles represent the peak maxima. The actual position of the low-energy edge E_{min} presumably occurs somewhere between.

Theory and experiment on Ag are summarized in Fig. 7. The full curve represents the variation with photon energy of E_{min} given by Eq. (21) using the parameters of Morris and Lynch.[17] The full circles denote the positions of the valley minima shown in Fig. 6 with some obtained at other photon energies and from different samples. The open circles correspond to position of peaks; the open squares correspond to position of peaks in Bauer's

FIG. 4. Geometry of the constant energy surfaces for optical transitions in the two-OPW approximation. The labeling is similar to that in Fig. 1. Transitions are permitted only on the disk whose diameter is given by FCF'.

data.[18] As with K, the nearly free-electron model seems to account well for the systematics of the observed structure. The same analysis has been performed on Cu with similar results.

V. FOUR-OPW: ALUMINUM

A. Band Structure

For the extension to the four-OPW case, we considered Al which is regarded as quite free-electron-like and whose band structure has been calculated by a number of authors.[21-24] We shall use here the fit to the Fermi surface data by Ashcroft.[22] The energy eigenvalues at a given point in $\vec{k}$ space are obtained by solving the secular determinant

$$\begin{vmatrix} T_1 - \mathcal{E} & V_{111} & V_{111} & V_{200} \\ V_{111} & T_2 - \mathcal{E} & V_{200} & V_{111} \\ V_{111} & V_{200} & T_3 - \mathcal{E} & V_{111} \\ V_{200} & V_{111} & V_{111} & T_4 - \mathcal{E} \end{vmatrix} = 0, \quad (23)$$

where

$$T_1 = \beta k^2, \quad T_2 = \beta (\vec{k} - \vec{G}_{200})^2,$$
$$T_3 = \beta (\vec{k} - \vec{G}_{111})^2, \quad T_4 = \beta (\vec{k} - \vec{G}_{11\bar{1}})^2, \quad (24)$$

and where V_{111} and V_{200} are appropriate pseudopotential coefficients taken from Ashcroft.[22]

Since the maximum photon energy in photoemission experiments is quite high (11.3 eV in currently available data on Al [9]), it was found that these four bands were insufficient. We therefore included three additional higher bands of the simple free-electron from, namely,

$$\mathcal{E}_5 = T_5 = \beta (\vec{k} - \vec{G}_{020})^2,$$
$$\mathcal{E}_6 = T_6 = \beta (\vec{k} - \vec{G}_{1\bar{1}\bar{1}})^2, \quad (25)$$
$$\mathcal{E}_7 = T_7 = \beta (\vec{k} - G_{1\bar{1}1})^2.$$

The algebra involved in the evaluation of the EDJDOS now becomes too cumbersome, so we have proceeded by numerical techniques. The method is essentially the same as that used by Brust[11] in calculations on Si.

B. Numerical Procedure

In numerical calculations, we have found it more convenient to work from the original definition of the EDJDOS of Eq. (3) rather than try to evaluate the line integral of Eq. (5). We have therefore evaluated $\mathfrak{D}(\mathcal{E}, \hbar\omega)$ for Al by sampling $\vec{k}$ space at about 289 000 points arranged on a cubic mesh in the $\frac{1}{48}$ symmetry sector of the Brillouin zone. At
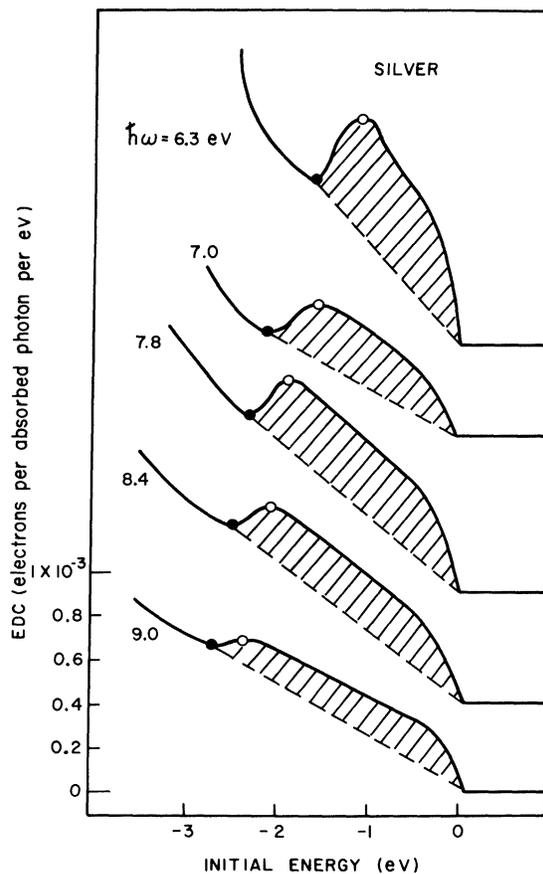
FIG. 6. The high-energy end of the experimental EDC's on cesiated Ag taken by Berglund and Spicer (Refs. 5 and 19). The curves are plotted against $E - \hbar\omega - E_F$, i.e., the initial-state energy, taking the zero of energy at the Fermi level.

each point, the seven energies described by Eqs. (23)–(25) were calculated. As pointed out by Ashcroft,[22] it is more economical in computer time to expand the determinant of Eq. (23) and solve the resulting quartic. We adopted this procedure. Having obtained the energy eigenvalues at this point in $\vec{k}$ space, the permitted optical transitions were deduced and dumped into "bins" which had been labeled according to photon energy and intial-state energy (the electron and photon energy scales were divided into intervals about 0.1 eV wide). Each transition was properly weighted with respect to the symmetry of the point in $\vec{k}$ space. After all points had been sampled, histograms were constructed from the contents of the bins. The density of states and the joint density of states were also computed by a similar histogram technique.

The reliability of the program was tested by first computing the EDJDOS for the case of perfectly free-electron bands. The results obtained numer-

ically can then be compared with those expected on the basis of the simple formulas derived in Sec. II. Figure 8 shows the free-electron EDJDOS for Al at $\hbar\omega = 10.7$ eV. The upper histogram of Fig. 8 corresponds to the internal distribution $\mathfrak{D}(\mathcal{E}, \hbar\omega)$. The lower historgam includes the escape factor as given in Eq. (7), and therefore represents the EDC of photoemitted electrons. (For this calculation the work function was taken to be 4.0 eV; the absorption coefficient was taken to be 10^6 cm^{-1} for photon energy range of interest; the electron mean free path was taken to vary as $(E - E_F)^{-1.5}$ and normalized at 50 Å for $E = E_F + 8.5$ eV.) The EDJDOS clearly shows the rectangular-box shape discussed earlier. There are, in fact, two distinct boxes. One arises from the $\langle 111 \rangle$ reciprocal-lattice vectors and the other from the $\langle 200 \rangle$ set. The low-energy steps correspond to the respective values of $E_{\min}$ defined by Eq. (14). The steps are of similar height, which is a consequence of attaching equal weight to all transitions. Because the EDJDOS is flat, the shape of the photoemitted EDC simply replicates the shape of the escape function.

The calculation was then repeated with the potential "switched on." The EDJDOS and EDC for $\hbar\omega = 10.7$ eV are shown in Fig. 9 and can be compared directly with Fig. 8. The over-all double-box feature is seen to persist but there is now significant additional structure. There are two prominent peaks of electrons labeled I and II at the high-energy end of the EDC, and a third (III) group of electrons at an intermediate energy. The low-energy group of electrons (IV), which is a remnant of the low-energy step of the free-electron box (one-

FIG. 8. The upper histogram is the free-electron EDJDOS for Al at $\hbar\omega = 10.7$ eV obtained by numerical methods. The lower histogram includes the escape factors and therefore represents the EDC of photoemitted electrons. The distributions are plotted against final-state energy taking the zero at the Fermi level. The vertical scale of the lower histogram has been magnified by an arbitrary scaling factor.

OPW), occurs below the vacuum level and is therefore inaccessible to experiment.

A series of photoelectron energy distributions is shown in Fig. 10 for a range of photon energies. The widths of the rectangular-box envelopes are seen to increase with increasing photon energy as expected. The substructure also shows some mino changes. However, only the three uppermost peaks emerge clearly above the vacuum level as can be seen in the EDC curves of Fig. 10 which include the escape factor (Figs. 8, 9, and 10 have

FIG. 7. Comparison of the theoretical values for $E_{\min}$ in Ag (full curve) with the positions of valley minima (full circles) and peaks (open circles) taken from Fig. 6. The open squares correspond to peaks in Bauer's clean Ag data.
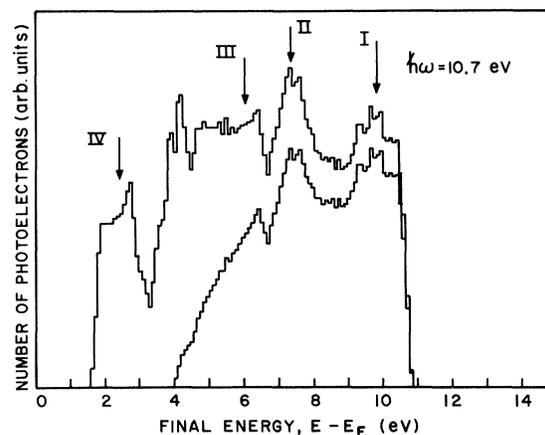
FIG. 9. The EDJDOS and the EDC of photoemitted electrons for Al at $\hbar\omega = 10.7$ eV in the four-OPW approximation. The scales are the same as in Fig. 8.
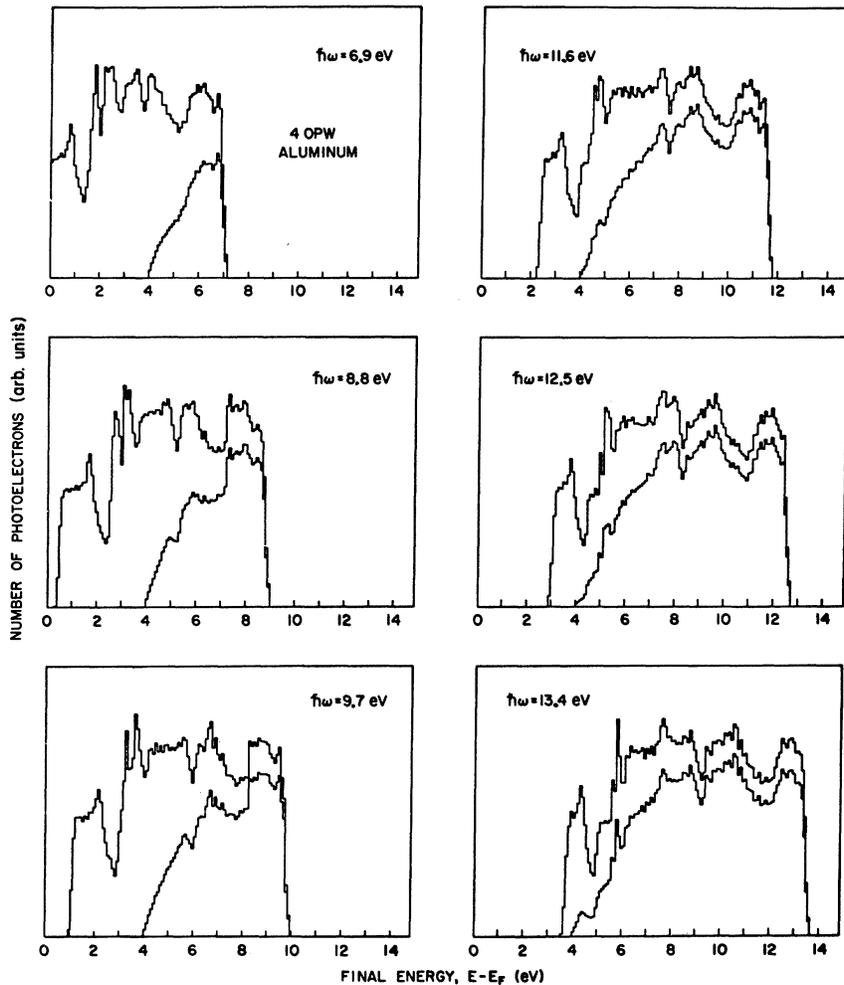
FIG. 10. The EDJDOS (upper histograms) and the EDC of photo-emitted electrons (lower histograms) for Al at various photon energies obtained in the four-OPW calculations. The scales are the same as in Fig. 8.

been broadened slightly by allowing a finite spread in the exciting photon energy with half-width of approximately 0. 2 eV.)

C. Comparison with Experiment

In order to make a better comparison with experiment, the calculated EDC's have been smoothed by convolving them with a Lorentzian broadening function whose width at half-maximum was 0. 28 eV. The smoothed curves are shown in Fig. 11 plotted against the initial-state energies. There are three pieces of structure labeled I, II, and III which are seen to superpose when referred to the initial states. This is just the behavior shown by the experimental curves of Wooten, Huen, and Stuart[9] which are plotted in Fig. 12. We conclude that the main features of the photoemission EDC's of Al can be successfully explained in terms of direct transitions using the known band structure. This is so in spite of our assumption of constant momentum matrix elements.

D. Relation to the Density of States

The two main features of the theoretical EDC's illustrated in Fig. 11 may be summarized as follows: (1) structure in the EDC's superposes when plotted against initial-state energy, and (2) the peaks show no abrupt changes in strength on varying the photon energy. These two features have previously been regarded as the prerogative of nondirect transitions, or direct transitions from very flat bands.[6] Indeed, the previous interpretations of the experiments on Al, and on the related metal In, [25] have invoked the nondirect model. Our calculations furnish an important counterexample of this rule since the bands of Al are quite wide.

In the nondirect model, the EDJDOS in Eq. (6) is replaced by a simple product of an initial and a final density of states

$$\mathcal{D}_{non}(\mathcal{E}, \hbar\omega) = \rho(\mathcal{E})\rho(\mathcal{E}+\hbar\omega) . \qquad (26)$$

The density of states for Al obtained in the present
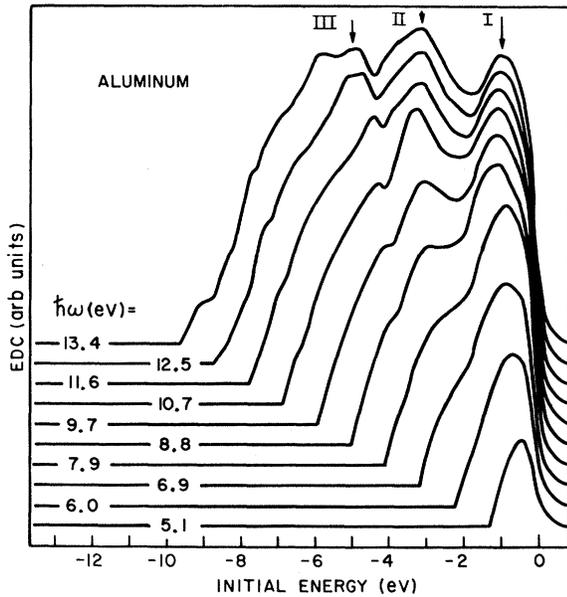
FIG. 11. Smoothed theoretical energy distribution curves of photoemitted electrons from Al, calculated from the four-OPW model. The curves are plotted against $E - \hbar\omega - E_F$, i.e., the initial-state energy with zero taken at the Fermi level.

FIG. 12. Experimental energy distribution curves of photoemitted electrons from Al measured by Wooten, Huen, and Stuart (Ref. 9) and plotted against initial-state energy as in Fig. 11.

calculation is shown in Fig. 13. It is seen that there are three pieces of structure in the density of states below the Fermi level. These are due to distortions of the energy surfaces at the zone boundaries. Above the Fermi level, the density of states is smooth and essentially free-electron-like.

If we calculate the EDC's using the nondirect Eq. (26) we inevitably obtain curves showing three peaks which superpose when plotted against initial-state energy, and which show no abrupt changes in strength on varying the photon energy. Moreover, these peaks coincide in energy location with the structure obtained using the direct-transition model. This is illustrated in Fig. 14, where we show the EDC at $\hbar\omega = 10.7$ eV calculated according to the direct and nondirect models. The experimental EDC of Wooten et al.[9] is also shown. Both the direct and the nondirect curves show the major features of the density of states, and agree reasonably well with experiment. Technically, therefore, the direct and nondirect models are indistinguishable. We are inclined to give the more conventional direct model the benefit of the doubt in such circumstances. Also, there is no theoretical reason to suppose that the transitions in a free-electron metal like Al should be nondirect. It has been argued by Spicer[6] and more recently by Doniach[26] that any nondirect behavior requires flat bands and the associated heavy mass.[27]

It is seen from Fig. 13 that the density of states

is smooth for energies below the three peaks. The EDJDOS, however, is rich in structure in this region as can be seen from Figs. 9 and 10. If we were able to probe this low-energy region, there is a good chance that we could distinguish unambiguously between the direct and nondirect models. One
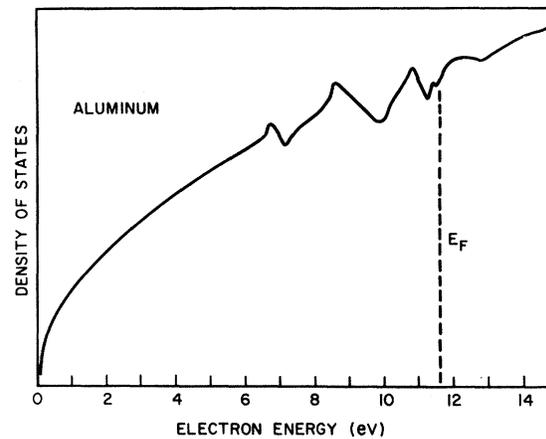
FIG. 13. Density of states of Al calculated from the four-OPW model. The zero of energy is taken at the bottom of the band.
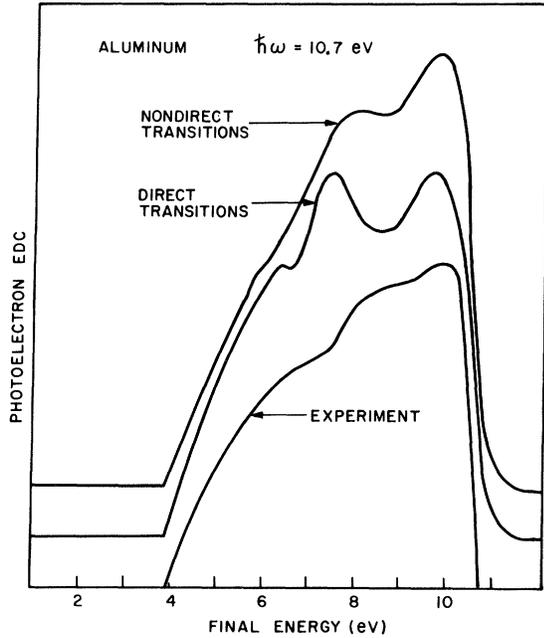
FIG. 14. Comparison of the direct and nondirect pre-
dictions with the experimental EDC at $\hbar\omega = 10.7$ eV. The
energy scale is the same as in Figs. 8–10.

approach would be to lower the work function by
cesiation. This has been attempted[28] but was un-
successful since the original EDC structure of the
clean Al was severely distorted by the Cs. Another
possibility would be to perform experiments at
higher photon energies, and thus excite the low-
lying structure to energies above the vacuum level.
Although we already opt for the direct-transition
interpretation, it would be highly desirable to have
this experimental confirmation.

VI. CONCLUSIONS

The predictions of the nearly free-electron model
for the photoemission behavior of simple metals
have been found to work encouragingly well for Na,
K, Rb, and Cs, for the conduction-band–to–conduc-
tion-band transitions in Ag and Cu, and for Al.
An analysis similar to that on Al has been per-
formed on In with comparable success and will be
reported elsewhere.[29]

An interesting result has been the similarity be-
tween the predictions of the direct and nondirect
models for Al. The differences and similarities of
the direct and nondirect models are summarized
very concisely by the following two equations:

$$\text{EDC (direct)} \propto \int \frac{dl_{fi}}{|\nabla_{\vec{k}}\mathscr{E}_f \times \nabla_{\vec{k}}\mathscr{E}_i|} , \qquad (27)$$

$$\text{EDC (nondirect)} \propto \left(\int \frac{dS_f}{|\nabla_{\vec{k}}\mathscr{E}_f|} \right) \times \left(\int \frac{dS_i}{|\nabla_{\vec{k}}\mathscr{E}_i|} \right) . \qquad (28)$$

Equation (28) is derived from (26) by expressing
the densities of states as integrals over the sur-
faces S_i and S_f of constant energy $\mathscr{E}_i$ and $\mathscr{E}_f$, respec-
tively. In the direct model, the EDC depends on
the EDJDOS, which in turn is given by the line in-
tegral in Eq. (27). The zeros of the denominator
in the integrand give rise to singularities. It is
tempting to do as Phillips does for the JDOS[10] and
try to categorize these singularities. We divide
them into two types.

Type A. Suppose that the line integral samples
a portion of $\vec{k}$ space in which either $|\nabla_{\vec{k}}\mathscr{E}_i|$ or
$|\nabla_{\vec{k}}\mathscr{E}_f|$ vanishes or is very small. This will tend
to give rise to a peak in the EDJDOS. Since the
surface integrals of (28) must sample the same re-
gion of $\vec{k}$ space, there is likely to be a peak also
in the density of states. In these circumstances,
the direct and nondirect pictures might look rather
similar. Clearly, there is no exact correspondence
here since the line integral constitutes a much more
restrictive sampling of $\vec{k}$ space than the surface in-
tegrals.

Type B. In this category, the gradients do not
vanish individually but their vector product does:

$$\left| \nabla_{\vec{k}}\mathscr{E}_f \times \nabla_{\vec{k}}\mathscr{E}_i \right| = 0, \quad \nabla_{\vec{k}}\mathscr{E}_f \neq 0, \quad \nabla_{\vec{k}}\mathscr{E}_i \neq 0. \qquad (29)$$

Structure in the EDJDOS due to singularities of this
kind has no counterpart in the nondirect model.
There will, therefore, be characteristic behavior
peculiar to direct transitions. For example, the
low-energy step in the EDJDOS at $E_{\min}$ discussed
in Secs. III and IV is due to a singularity of this
type. An analysis of this and other kinds of critical
point behavior has been given recently by Kane.[30]

It is to be noted that Al is a good candidate for
structure of type A. The Fermi surface is large and
overlaps into several zones. The energy surfaces
in the vicinity of the Fermi level are therefore in-
tersected by many zone boundaries, so that there
are many regions of $\vec{k}$ space for which $|\nabla_{\vec{k}}\mathscr{E}_f|$ and
$|\nabla_{\vec{k}}\mathscr{E}_i|$ are small. The direct and nondirect pre-
dictions might therefore be expected to be similar
expecially at the high-energy end of the EDC's.
While the foregoing argument is far from exact, it
does provide some retrospective insight into simi-
larities which can occur between the direct and non-
direct models.

*Part of this work was performed while one of the authors (N. V. S.) was a research associate at Stanford University and part while on assignment at Stanford from Bell Telephone Laboratories. The work at Stanford was supported in part by U. S. Army Engineer Research and Development Laboratories, Fort Belvoir, Va., Contract No. DA-44-009-AMC1474(7), by the Advanced Research Projects Agency through the Center for Materials Research at Stanford University, and by the National Science Foundation.

†Present address: National Bureau of Standards, Washington, D. C. 20234.

‡Permanent address.

[1]A. H. Wilson, *Theory of Metals* (Cambridge U. P., New York, 1936), p. 135.

[2]P. N. Butcher, Proc. Phys. Soc. (London) A64, 50 (1951).

[3]A. I. Golovashkin, A. I. Kopeliovich, and G. P. Motulevich, Zh. Eksperim. i Teor. Fiz. 53, 2253 (1968) [Soviet Phys. JETP 26, 1161 (1968)].

[4]W. E. Spicer, Phys. Rev. 112, 114 (1958).

[5]C. N. Berglund and W. E. Spicer, Phys. Rev. 136, A1030, (1964); 136, A1044 (1964).

[6]W. E. Spicer, Phys. Rev. 154, 385 (1967).

[7]W. A. Harrison, *Pseudopotentials in the Theory of Metals* (Benjamin, New York, 1966).

[8]N. V. Smith and W. E. Spicer, Phys. Rev. 188, 593 (1959).

[9]F. Wooten, T. Huen, and R. Stuart, in *Proceedings of the International Colloquium on Optical Properties and Electronic Structure of Metals and Alloys, Paris 1965*, edited by F. Abelés (North-Holland, Amsterdam, 1966), p. 333.

[10]J. C. Phillips, in *Solid State Physics*, edited by F. Seitz and D. Turnbull (Academic, New York, 1966), Vol. 18, p. 55.

[11]D. Brust, Phys. Rev. 139, A489 (1965).

[12]S. Methfessel, Z. Physik 147, 442 (1957).

[13]H. Mayer and H. Thomas, Z. Physik 147, 419 (1957).

[14]N. V. Smith and G. B. Fisher (unpublished).

[15]N. F. Mott and H. Jones, *The Theory of the Properties of Metals and Alloys* (Dover, New York, 1958), p. 64.

[16]See, for example, Ref. 3. Equation (22) is exact and does not depend on one of the plane-wave components being treated as small in amplitude compared to the other.

[17]C. E. Morris and D. W. Lynch, Phys. Rev. 182, 719 (1969).

[18]R. S. Bauer (private communication).

[19]The curves in Fig. 6 showing Berglund and Spicer's data on Ag were taken from W. F. Krolikowski's thesis [Stanford University, 1967 (unpublished)] where they are presented in greater detail than in Berglund and Spicer's original paper (Ref. 5).

[20]The background is possibly due to electrons which have undergone an inelastic electron-electron scattering. It is to be noted that the subtraction used here is different from that used originally by Berglund and Spicer (Ref. 5) in their work on Cu and Ag. It is not clear which is correct.

[21]W. A. Harrison, Phys. Rev. 118, 1182 (1960).

[22]N. W. Ashcroft, Phil. Mag. 8, 2055 (1963).

[23]B. Segall, Phys. Rev. 124, 1797 (1961).

[24]E. C. Snow, Phys. Rev. 158, 683 (1967).

[25]R. Y. Koyama, W. E. Spicer, N. W. Ashcroft, and W. E. Lawrence, Phys. Rev. Letters 19, 1284 (1967).

[26]S. Doniach (unpublished).

[27]Even in the d-band metals, the need to invoke nondirect transitions does not seem as strong as it once did. This has been demonstrated in recent work by N. V. Smith and W. E. Spicer, Opt. Commun. 1, 157 (1969); N. V. Smith, Phys. Rev. Letters 23, 1452 (1969); P.-O. Nilsson, C. Norris, and L. Wallden, Solid State Commun. 7, 1705 (1969); D. E. Eastman and J. K. Cashion, Phys. Rev. Letters 24, 310 (1970).

[28]N. V. Smith and R. Y. Koyama (unpublished).

[29]R. Y. Koyama and W. E. Spicer (unpublished).

[30]E. O. Kane, Phys. Rev. 175, 1039 (1968).